



HAL
open science

Cd content dependent structural and magnetic properties of Cd-Ni nano ferrite

Rulan Verma, Shashank Kane, Priyanka Tiwari, Frédéric Mazaleyrat

► **To cite this version:**

Rulan Verma, Shashank Kane, Priyanka Tiwari, Frédéric Mazaleyrat. Cd content dependent structural and magnetic properties of Cd-Ni nano ferrite. *Advances in basic Science (ICABS 2019)*, Feb 2019, Bahal, India. pp.160001, 10.1063/1.5122582 . hal-04452705

HAL Id: hal-04452705

<https://hal.science/hal-04452705>

Submitted on 12 Feb 2024

HAL is a multi-disciplinary open access archive for the deposit and dissemination of scientific research documents, whether they are published or not. The documents may come from teaching and research institutions in France or abroad, or from public or private research centers.

L'archive ouverte pluridisciplinaire **HAL**, est destinée au dépôt et à la diffusion de documents scientifiques de niveau recherche, publiés ou non, émanant des établissements d'enseignement et de recherche français ou étrangers, des laboratoires publics ou privés.

Copyright

RESEARCH ARTICLE | AUGUST 29 2019

Cd content dependent structural and magnetic properties of Cd-Ni nano ferrite

R. Verma; S. N. Kane ; P. Tiwari; F. Mazaleyrat

 Check for updates

AIP Conf. Proc. 2142, 160001 (2019)

<https://doi.org/10.1063/1.5122582>



View
Online



Export
Citation

CrossMark



Cut Hall measurement time in *half*
using an M91 FastHall™ controller



Also available as part of a tabletop system and an option for your PPMS® system

Cd Content Dependent Structural And Magnetic Properties Of Cd-Ni Nano Ferrite

R. Verma¹, S. N. Kane^{1, a)}, P. Tiwari^{1,2}, and F. Mazaleyrat³

¹Magnetic Materials Laboratory, School of Physics, D. A. University, Khandwa road, Indore – 452001, India.

²Department of Physics, Prestige Institute of Engineering Management and Research, Indore - 452010, India.

³SATIE, ENS Universite Paris-Saclay, CNRS 8029, 61 Av. du Pdt. Wilson, F-94230, Cachan, France.

^{a)} Corresponding author: kane_sn@yahoo.com

Abstract. Ni_{1-x}Cd_xFe₂O₄ (0.0 ≤ x ≤ 0.72) ferrites were synthesized by sol-gel auto-combustion method. X-ray diffraction, magnetic measurements were used to investigate structural, magnetic properties of nanocrystalline ferrite with Scherrer's grain diameter (*D*) ranging between 9.67 – 38.27 nm. Results reveal that with increasing Cd content, there is an increase of experimental lattice parameter (*a_{exp}*), x-ray density (*ρ_{XRD}*), specific surface area (*S*), and hopping lengths for tetrahedral and octahedral site (*L_A*, *L_B*), accounted for difference in ionic radii of Cd²⁺ (0.097 nm) as compared to the Ni²⁺ ion (0.069 nm) and Fe³⁺ ion (0.064 nm). With Cd²⁺ ions addition: a) they remain more populated on A site, Ni²⁺ ions remain more populated on B site, whereas concentration of Fe³⁺ ions increases on B-site, resulting in increasing saturation magnetization (*M_s*) from 30.2 – 54.4 Am²/kg; b) distribution of Ni²⁺, Cd²⁺, Fe³⁺ cations on tetrahedral (A) and octahedral (B) site shows mixed spinel structure; c) oxygen positional parameter (*u*), inversion parameter (*δ*) also display increase of disorder, degree of inversion, affecting *M_s* and coercivity (*H_c*) (varies between 73.2 – 198.9 Oe).

INTRODUCTION, EXPERIMENTAL DETAILS, AND DATA ANALYSIS

Spinel ferrites have a general formula Me²⁺O.Fe³⁺₂O₃ (where Me represent divalent ions Mg²⁺, Zn²⁺, Ni²⁺ etc.), are technologically important owing to their interesting structural, magnetic properties [1]. Nanosized spinel ferrites have attracted considerable attention for their use in microwave devices, high speed digital tape, ferrofluids, and as catalyst. Spinel ferrites have Fd_{3m} space group reveal fcc (face centered cubic) structure, with total 56 ions per unit cell, 32 divalent oxygen ions forms closed pack fcc structure with 64 tetrahedral interstitial sites (*A-sites*) and 32 octahedral interstitial sites (*B-sites*), out of available sites only 8 tetrahedral (*A-sites*) and 16 octahedral (*B-sites*) are occupied by divalent and trivalent metal ions [2], thus, large fraction of unoccupied interstitial sites in the spinel ferrites promote their filling with appropriate divalent cations allowing the possibility to fine tune their magnetic behavior [3]. It is known that the structural, magnetic properties of spinel ferrites depend on choice of cations, type of additives, synthesis technique, thermal treatment, and distributions of cations between tetrahedral (A-site) and octahedral (B-site) [4]. Ni ferrite (NFO) has inverse spinel structure, where Ni²⁺ ions are located on octahedral (B-site) site. Gradual substitution in NFO with an element, known to form normal spinel would transform the substituted ferrite from inverse to normal via mixed spinel structure. Substitution induced changes in cationic distribution, would even lead to non-equilibrium site occupancy observed in nano-structured ferrites [4,5], allows the possibility to tailor the magnetic properties. Literature shows that mixed CdFe₂O₄ ferrite shows normal spinel structure with Cd²⁺ ions have a preference on tetrahedral (A-site), is technologically important due to its resistivity, high permeability, low magnetic losses [4]. Addition of Cd²⁺ ion in NFO, modifies the magnetic properties e.g. – saturation magnetization coercivity etc. [5]. Studies report structural, magnetic properties of Co-Cd [6], Ni-Cu-Cd [7], Li-Cd [8] mixed ferrite prepared by using various methods e.g. - double sintering ceramic technique [6], coprecipitation technique [7], and microwave combustion technique [8]. However, study on structural, magnetic properties of Ni-Cd ferrites using sol-gel auto-combustion method is rather less explored. Advantage of sol-gel

auto-combustion synthesis is: formation of spinel structure even in dry gel form [9], so high temperature sintering may not be needed for the formation of spinel phase. Thus, it is one of the most proficient methods, for synthesizing nano-materials at relatively lower temperature making this technique energy efficient, with increased surface area maintaining the quality of material. Therefore, in the present work x-ray diffraction (XRD), magnetic measurements were used to probe structural, magnetic properties of $\text{Ni}_{1-x}\text{Cd}_x\text{Fe}_2\text{O}_4$ ($0.0 \leq x \leq 0.72$) ferrites, prepared by sol-gel auto-combustion method.

$\text{Ni}_{1-x}\text{Cd}_x\text{Fe}_2\text{O}_4$ ($x = 0.0 \leq x \leq 0.72$) ferrites were produced by sol-gel auto-combustion method, by mixing AR grade: [Nikel acetate – $(\text{CH}_3\text{COO})_2\text{Ni} \cdot 4\text{H}_2\text{O}$], Cadmium acetate – $(\text{CH}_3\text{COO})_2\text{Cd} \cdot 2\text{H}_2\text{O}$], Ferric nitrate – $(\text{Fe}(\text{NO}_3)_3 \cdot 9\text{H}_2\text{O})$] in stoichiometric ratio. Citric acid was also added by maintaining its ratio with metal salt as 1:1, which acts as a chelating agent, as well as fuel in combustion process. All precursors were dissolved in deionized water, and then ammonia solution (NH_4OH) was added to maintain the pH at 7. Solution was heated at $\sim 110^\circ\text{C}$ in air until fluffy powder called as ‘dry gel’ was formed, which was heat treated at 600°C for 3 hours. Annealed ferrites were characterized by XRD measurements, done at room temperature in $\theta - 2\theta$ configuration by Bruker D8 advance diffractometer by $\text{CuK}\alpha$ radiation ($\lambda = 0.154056$ nm), utilizing Bruker LynxEye detector for detecting x-rays. Rietveld refinement of XRD patterns was done by MAUD (Material Analysis Using Diffraction) software [12] to calculate experimental lattice parameter (a_{exp}). Specific surface area (S) was calculated using the expression: $S = [6 / (D \times \rho_{\text{XRD}})]$ [11], X-ray density (ρ_{XRD}) of the studied samples was obtained by: $\rho_{\text{XRD}} = 8M_w/N(a)^3$ where M_w – Molecular weight, N – Avagadro’s number, a – Lattice parameter. Scherrer’s grain diameter (D) is obtained by using the line width of [311] reflection via expression: $D = 0.9 \lambda / \beta \cos\theta$ where, λ - wavelength of the x-ray used, β - line width, θ - peak position (in 2θ scale). Hopping length for site A, B was calculated by: $L_A = (\sqrt{3}/4) a$, $L_B = (\sqrt{2}/4) a$, where L_A , L_B are respectively hopping length for site A, B, a – lattice parameter. XRD peak intensities were used to obtain cation distribution of the studied samples, employing Bertaut method as described in [13-15], used to calculate theoretical lattice parameter (a_{th}). Néel magnetic moment ‘ n_N ’ or ‘ $M_{s(t)}$ ’ (theoretical magnetic moment at 0 K) is calculated by: $n_N = M_B - M_A$, where M_A , M_B respectively are magnetic moment of A, B-site. Ionic radii of A, B site (r_A , r_B), oxygen parameter (u), bond angles (θ_1 , θ_2 , θ_3 , θ_4 , θ_5), tetrahedral, octahedral bond length (R_A , R_B) were estimated from cation distribution. Room temperature hysteresis loops were measured by Lakeshore Model 7410 (VSM) by applying maximum field - $H_{\text{max}} \approx 1.9$ T, were used to get coercivity (H_c), saturation magnetization ($M_{s(\text{exp})}$).

RESULTS AND DISCUSSIONS

XRD patterns of the annealed $\text{Ni}_{1-x}\text{Cd}_x\text{Fe}_2\text{O}_4$ ($x = 0.0 \leq x \leq 0.72$) ferrites are shown in figure 1a. XRD confirms the formation of spinel ferrite. Minor presence of secondary phase $\alpha\text{-Fe}_2\text{O}_3$ (for sample with $x = 0.0$) is also observed. Rietveld refinement of samples for $x = 0.24$, $x = 0.36$ are respectively shown in figure 1 b, c. Table 1 depicts the calculated values of a_{exp} , D , ρ_{XRD} , cell volume V , S , L_A , and L_B for the studied samples. Perusal of table 1 shows increase of a_{exp} , V , ρ_{XRD} , S , L_A , L_B with increasing Cd^{2+} content, attributed to the dissimilar ionic radii of Ni^{2+} , Cd^{2+} . Figure 2 a shows experimental lattice parameter a_{exp} and ρ_{XRD} (inset of fig. 2a) increases linearly with increasing Cd^{2+} content, ascribed to the addition of an ion with higher ionic radius ($\text{Cd}^{2+} = 0.097$ nm) for an ion which has lower ionic radius ($\text{Ni}^{2+} = 0.069$ nm). Linear increase of lattice parameter with Cd^{2+} content shows that Cd^{2+} ions enter into the spinel lattice.

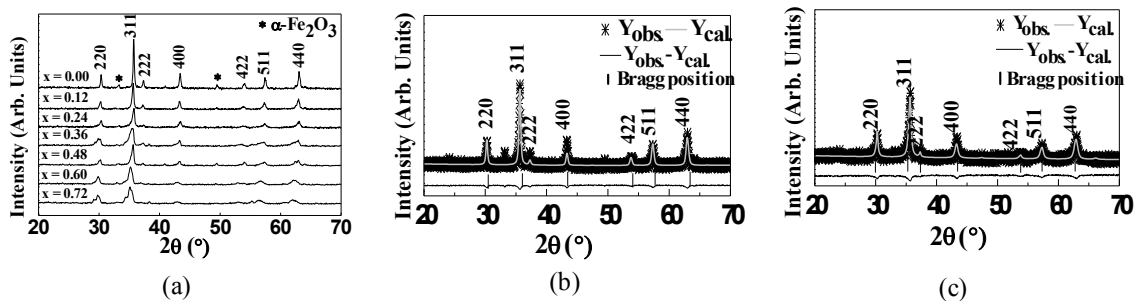


FIGURE 1. (a) XRD patterns of the studied $\text{Ni}_{1-x}\text{Cd}_x\text{Fe}_2\text{O}_4$ ferrites, (b) and (c) Rietveld refinement for $x = 0.24$, $x = 0.36$

Table 1. Compositional dependence of experimental lattice parameter (a_{exp}), grain diameter (D), cell volume (V), x-ray density (ρ_{XRD}), specific surface area (S) and hopping length for A-site, B-site (L_A, L_B) for the studied samples.

x	a_{exp} nm	D nm	V (nm ³)	ρ_{XRD} (kg/m ³)	S (m ² /g)	L_A (nm)	L_B (nm)
0.0	0.8329	38.27	0.5779	5387.2	29.10	0.3606	0.2948
0.12	0.8355	27.65	0.5832	5485.1	39.55	0.3617	0.2957
0.24	0.8334	20.96	0.5789	5673.6	50.44	0.3608	0.2950
0.36	0.8410	10.24	0.5948	5665.8	103.38	0.3641	0.2977
0.48	0.8366	19.90	0.5855	5901.9	55.81	0.3622	0.2961
0.60	0.8452	12.97	0.6039	5864.2	78.88	0.3659	0.2992
0.72	0.8464	09.67	0.6064	5980.3	103.64	0.3665	0.2996

Increase of unit cell volume ' V ' (shown in table 1), displays increase of unit cell mass, accountable for the higher value of ρ_{XRD} can be attributed to the replacement of an ion with lower mass (Ni = 58.71 g/mol) by Cd²⁺ ion with higher mass (Cd = 112.40 g/mol). Average grain diameter ' D ' range between 09.67 nm – 38.27 nm, displays decrease with increasing Cd²⁺ content, is understood in terms of increase of Cd²⁺ ion in the unit cell, which has higher ionic radius would result in grain boundary dispersion, thus hindering the grain growth. Figure 2 b, displays the Cd²⁺ content dependence of ionic radii of A and B-site (r_A, r_B), bond length (R_A, R_B), shared tetrahedral, octahedral, and unshared octahedral edges (d_{AXE}, d_{BXE}). Perusal of fig. 2 b shows that changes in ionic radii, bond length of A site increases, A site will expand in such way that anions associated with A-site will move away from each other, as a result the distance between d_{AXE} and R_A would increase. Similarly as r_B decreases, the values of d_{BXE} and R_B would also decrease. Increase of Cd²⁺ content in the studied samples leads to higher specific surface area ' S ' (shows linear variation Cd²⁺ content, varies between 29.10 – 103.64 m²/g, implies more porosity, which is attractive for catalytic activity of the studied samples. Higher surface area implies small grain diameter because there is inverse relationship between D and ρ_{XRD} with specific surface area, seen clearly in table 1. Both hopping lengths for A, B-site (L_A, L_B) display similar trend as that of a_{exp} . Perusal of figure 2 (c) shows linear variation of M_s with inversion parameter δ , shows M_s enhancement up to 1.8 times (from 30.2 – 54.5 Am²/kg). Based on variation between M_s, δ , following empirical relation can be written: $M_s = A \delta + B$, where A, B are fitting constants with values respectively 46.1, 36.1. It is to be mentioned that the empirical relation is just to show linear relation between M_s, δ . This variation clearly shows that δ contributes decisively in determining M_s of the studied samples.

Table 2, gives distribution of cations on A, B site, δ , u^{43m} for the studied Ni_{1-x}Cd_xFe₂O₄ ($x = 0.0 \leq x \leq 0.72$) nano ferrites. Perusal of table 2 shows changes in inversion parameter (δ), oxygen position parameter (u^{43m}) with increasing Cd²⁺ content. Increase of ' u^{43m} ' values from 0.3797 to 0.3852 (which is higher than the ideal value of 0.375 for Ni-Cd nano-ferrites) suggests that the movement of O²⁻ ions in such a way that distance between A-O ions (tetrahedral bond length R_A) increases, ascribed to the replacement of cation on A-site. With increasing Cd²⁺ doping Ni²⁺ ions remain Ni²⁺ and Fe³⁺ ions become more populated on B-site, whereas Cd²⁺ ions remain distributed, predominantly on A site, thus increasing the value of δ .

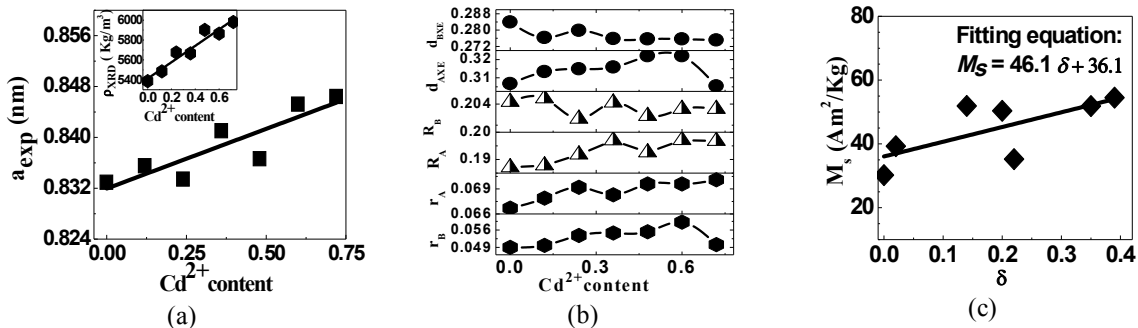


FIGURE 2. (a) Cd²⁺ dependent a_{exp} . Inset: Cd²⁺ dependent ρ_{XRD} , (b) Cd²⁺ content dependence of $r_A, r_B, R_A, R_B, d_{AXE}, d_{BXE}$ (c) M_s variation with δ Continuous lines are linear fit to the data

Table 2. Compositional dependence of Cation distribution (for A, B site), inversion parameter (δ), oxygen parameter (u), with Cd content.

x	Cation distributions		δ	u
	A-Site	B-Site		
0.0	(Ni _{0.01} Fe _{0.99}) ^A	[Ni _{0.99} Fe _{1.01}] ^B	0.00	0.3797
0.12	(Ni _{0.05} Cd _{0.02} Fe _{0.93}) ^A	[Ni _{0.83} Cd _{0.10} Fe _{1.07}] ^B	0.02	0.3798
0.24	(Ni _{0.13} Cd _{0.14} Fe _{0.73}) ^A	[Ni _{0.63} Cd _{0.22} Fe _{1.15}] ^B	0.14	0.3829
0.36	(Ni _{0.00} Cd _{0.20} Fe _{0.80}) ^A	[Ni _{0.64} Cd _{0.16} Fe _{1.20}] ^B	0.20	0.3823
0.48	(Ni _{0.0} Cd _{0.22} Fe _{0.78}) ^A	[Ni _{0.52} Cd _{0.26} Fe _{1.22}] ^B	0.22	0.3834
0.60	(Ni _{0.01} Cd _{0.35} Fe _{0.64}) ^A	[Ni _{0.59} Cd _{0.25} Fe _{1.16}] ^B	0.35	0.3847
0.72	(Ni _{0.00} Cd _{0.39} Fe _{0.61}) ^A	[Ni _{0.28} Cd _{0.33} Fe _{1.39}] ^B	0.39	0.3852

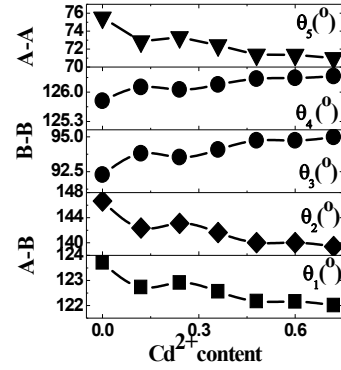


FIGURE 3. Compositional dependence of bond angles

By adding Cd²⁺ ion, ionic radii, bond lengths of A, B sites get modified in such a way that distortion in the structure increases, as evidenced by changes in u values, shown in table 2, and would get reflected in magnetic properties, as explained later.

Perusal of table 2 also shows that with increasing Cd content, u also increases confirming increased distortion in the spinel structure, responsible for observed M_s increase, as was also observed earlier [15], and also demonstrates the significance of cationic distribution (on A, B site) in determining magnetic properties.

Magnetic exchange strength (A-O-B, A-O-A, B-O-B) not only depends on bond angles, but also on bond lengths. Cd-content dependence of bond angles ($\theta_1, \theta_2, \theta_3, \theta_4, \theta_5$) provides information on A-O-B, A-O-A, B-O-B exchange interaction, is shown in fig.3. Perusal of figure 3 clearly shows Cd dependent changes in bond angles lead to weakening of A-A, A-B interaction with simultaneous strengthening of B-B interaction [16,17], reflected in changes in magnetic properties, as shown in figure 3.

Figure 4 (a) depicts the room temperature hysteresis loops of the studied samples, display composition dependent changes in magnetic properties. Figure 4 (b) depicts the grain size dependence of H_c , and Cd²⁺ content dependence of H_c (shown as inset). Perusal of fig. 4 (b) shows that H_c , i) decreases linearly by increasing Cd²⁺ content in the sample, and ii) increases linearly with increasing grain size. Observed H_c dependence on D , indicates that the studied samples lie in the region with overlap between single, and multi domain region [18].

Figure 4 (c) depicts the Cd²⁺ content dependence of experimental saturation magnetization M_s (M_s (exp)), and theoretical magnetization at 0 K: M_s (M_s (t)) (also known as Néel magnetic moment) for the studied samples. Observed changes are attributed to variation in cationic distribution, as shown in table 2. Overall increase of magnetic ions (Ni²⁺, Fe³⁺ ions) on B-site leads to increase of net magnetic moment, explains increase of both M_s (M_s (t)), M_s (exp) as shown in figure 4 (c). For the studied samples, observed similar trend of M_s (exp), M_s (t) shows that the magnetization behavior of the studied samples is governed by Néel model [12-19], demonstrating strong correlation between magnetic, structural properties.

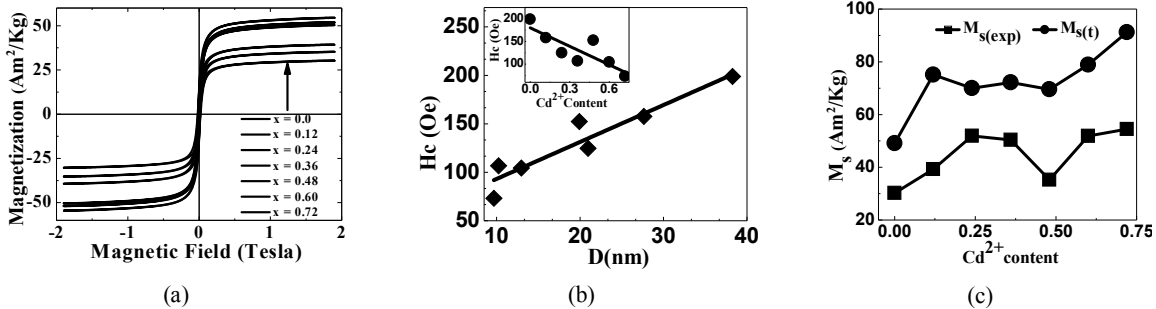


FIGURE 4. (a) Hysteresis loops of the studied samples, (b) H_c variation with D . Inset: Cd²⁺ dependence of H_c . Continuous lines are linear fit to the data, (c) Variation of experimental M_s (exp), M_s (t) with Cd²⁺ content

SUMMARY

We report the sol-gel auto-combustion synthesis of Ni-Cd ferrites with different cadmium concentration. XRD confirms the formation of nano-sized spinel ferrite. Increase in Cd^{2+} content leads to : i) Linear increase of lattice parameter and reveals that Cd^{2+} ions enter into the spinel lattice, ii) decrease of grain diameter, shows that increasing Cd^{2+} content in the sample, hinders the grain growth, iii) Ni^{2+} , Fe^{3+} ions remain more populated on B-site, whereas Cd^{2+} ions remain distributed, pre-dominantly on A site, thus increasing δ values, leading to increase of net magnetic moment, so increasing both M_s (t), M_s (exp), iv) an empirical relation between M_s , δ , is obtained, shows linear variation between them, v) weakening of A-A, A-B interaction with concurrent strengthening of B - B interaction, is responsible for observed changes in magnetic properties, vi) H_c decreases linearly with increasing Cd^{2+} content (H_c increases linearly with increasing grain size). Observed variation of H_c with D indicate that the studied samples lie in the region with overlap between single and multi domain region, and the magnetization behavior of the studied samples is governed by Néel model.

ACKNOWLEDGMENTS

Authors thank Dr. M. Gupta, UGC-DAE CSR, Indore for providing XRD data. SNK acknowledges gratefully one month invited professorship at ENS Paris-Saclay, Cachan (France), during Oct. - Nov. 2017.

REFERENCES

1. S. N. Kane, S. Raguwanshi, M. Satalkar, V. R. Reddy, U. P. Deshpande, T. R. Tatarchuk and F. Mazaleyrat, [AIP Conf. Proc.](#) **1953**, 030089-4 (2017)
2. P. B. Belavi, G. N., L. R. Naik, R. Somashekar, R. K. Kotnala, [Materials Chemistry and Physics](#) **132**, 138-144 (2012).
3. S. N. Kane, S. Raguwanshi, M. Satalkar, V. R. Reddy, U. P. Deshpande, T. R. Tatarchuk and F. Mazaleyrat, [AIP Conf. Proc.](#) **1953**, 030089-4 (2018).
4. S. K. Nath, K. H. Maria, S. Noor, S. S. Sikder, S. Manjura Hoque, M. A. Hakim, [Journal of Magnetism and Magnetic Materials](#) **324**, 2116-2120 (2012).
5. S. Singhal, S. Jauhar, K. Chandra and Sandeep Bansal, [Bull. Mater. Sci.](#), **36**, 107–114 (2013).
6. R. Suresh, P. Moganavally, M. Deepa, (IOSR) Journal of Applied Chemistry, **8**, 01-05 (2015).
7. S.C. Watawe, S. Keluskar, Gonbare, R. Tangsali, [Thin Solid Films](#) **505**, 168 – 172 (2006).
8. A. Sutka and G. Mezinskis, [Front. Mater. Sci.](#) **6(2)**, 128–141 (2012).
9. M. R. Patil, M. K. Rendale, S. N. Mathad, and R. B. Pujar, Inorganic And Nano-Metal Chemistry 1–5 (2017).
10. S. P. Jadhava; B. G. Toksha; K. M. Jadhav; N. D. Shinde, [Chin. J. Chem. Phys.](#), **23**, 4 (2010).
11. E. F. Bertaut, [C. R. Acad. Sci.](#) **230**, 213 (1950).
12. L. Gastaldi and A. Lapicciarella, [J. Solid State Chem.](#) **30**, 223 (1979).
13. M. Rahimi, M. Eshraghi, and P. Kamel, [Ceramics International](#), **40**, 15569–15575 (2014).
14. J. Smit, H. P. J. Wijn, [Ferites](#) (Philips Technical Library, Eindhoven, (1959).
15. S. Raghuvanshi, F. Mazaleyrat, and S. N. Kane, [AIP ADVANCES](#) **8**, (2018) 047804.
16. A. Ande, S. Thatikonda, R. Dachevall, V. Chinnala, S. Reddy, N. Rao Koppera, P. Meesala, [World Journal of Condensed Matter Physics](#), **2**, 257-266 (2012).
17. M. Satalkar, S. N. Kane, M. Kumaresavanji, J. P. Araujo, [Material Research Bulletin](#), **91**, 14-21 (2017).
18. A. G. Kolhatkar, A. C. Jamison, D. Litvinov, R.C. Willson, and T. Randall Lee, [Int. J. Mol. Sci.](#) **14**, 15977 (2013).
19. De Manojit, A. Mukherjee, H. S. Tewari, [Processing and Application of Ceramics](#) **9 [4]**, 193–197 (2015).